Airfoil Trailing-Edge Flow Measurements

Thomas F. Brooks* and Michael A. Marcolini*
NASA Langley Research Center, Hampton, Virginia
and
Dennis S. Pope†
Kentron International Inc., Hampton, Virginia

Trailing-edge data for boundary-layer/near-wake thickness parameters are given for airfoils and flat plates. Reynolds number effects are examined as a function of model size, velocity and boundary-layer tripping. Reference comparisons are made with boundary-layer calculations using potential-flow modeling and a finite-difference method for laminar and turbulent boundary layers. Open wind-tunnel corrections to angle of attack and camber are incorporated into the potential-flow modeling. It was found that the open tunnel flow turbulence affects early boundary-layer transition for the higher velocities. The theory still "brackets" the data allowing some assessment of boundary-layer transition behavior.

Introduction

THE knowledge of the flow at the trailing edge (TE) and near-wake region of an airfoil is very important, because it influences, or in another view is the result of, the entire flowfield of the airfoil. There is a need for detailed measurements in order to evaluate boundary-layer (BL) and wake-prediction capabilities with regard to BL approximations and/or turbulence modeling.[1,2] Previous trailing-edge measurements[1] have dealt with larger flat-plate models for very limited velocity ranges.

In addition to purely aerodynamic considerations there is interest in TE flow conditions from the standpoint of aeroacoustics. Studies[3] made to quantify airfoil self-noise in terms of flow parameters have required the measurement of trailing-edge flows to correspond to acoustic measurements.

The present paper presents trailing-edge flow data for a number of two-dimensional airfoil and flat-plate sections of various chord lengths, low-subsonic flow velocities, boundary-layer tripping, and angles of attack. The Reynolds number (*Re*) ranges from about 0.05×10^6 to almost 3×10^6 as based on the chord. This represents an expansion over that given by Brooks and Marcolini[3] for the BL/near-wake parameters, especially as a function of the angle of attack at various *Re*.

To help guide interpretation, the data are compared to theoretical results which incorporate inviscid potential-flow modeling and a well-documented boundary-layer differential method.[4] For the nonzero angle-of-attack cases, the potential-flow calculations incorporate theoretical open wind-tunnel corrections.[5] This is done to account for the flow conditions and pressure distributions of the airfoil in the tunnel as opposed to free-flow conditions. The use of calculated rather than measured pressures and the lack of direct knowledge of the transition locations, as well as the extent and structure of the transitional flow, prevent the theoretical comparisons with data from being interpreted as evaluations of the boundary-layer code. However, the comparisons demonstrate a bounded range of data one might expect when given normal geometry and flow conditions as input to theory. Consideration is given to transition criteria as to how they affect the boundary-layer parameter calculations for the trailing edge.

Presented as Paper 84-2266 at the AIAA/NASA Ninth Aeroacoustics Conference, Williamsburg, VA, Oct. 15-17, 1984; received Nov. 5, 1984; revision received Dec. 20, 1985.

*Research Scientist.

†Acoustics Engineer.

Theoretical Comparisons

Boundary-Layer Code

The boundary-layer program used is that of Harris and Blanchard.[4] The finite-difference program solves the nonsimilar boundary-layer equations for laminar, transitional, and turbulent flows. For the present use, the surface-pressure specification input for the program is obtained from inviscid potential-flow calculations of the Blade Section Aerodynamics module of the Aircraft Noise Prediction Program (ANOPP).[6] This module uses Theodorsen's method for arbitrary airfoils for the flow calculations. As will be discussed subsequently, the airfoil surfaces are defined by numerically determined "free-equivalent" airfoil mean-camber lines with sectional thickness added. The transition locations for the boundary-layer code must be specified as well as the end of transition locations. For smooth surfaces, transition would generally lie[7] between the points of instability and laminar separation.

In the present application, the input to the codes is approximate in that the surface pressures were not measured and no determination was made of the transition location or extent and structure of the transitional flow. It was decided that the most useful approach for the theoretical comparisons would be to "bracket" the data by presenting dual results as based on different boundary-layer transitional assumptions. One assumption is that fully turbulent flow began at the leading-edge region. The other is that fully turbulent flow starts upstream of the laminar separation location by a distance of 10% airfoil chord (thereby preventing separation). The Harris code does not contain a wake model. The effect of the airfoil wake is taken into account here by a smoothing of the streamwise pressure gradient near the trailing edge of the airfoil. This view is supported by Ref. 8.

Wind-Tunnel Corrections

In Ref. 5, classical methods were used with lifting-surface theory to obtain two-dimensional, open wind-tunnel corrections. Taken into account was the induced curvature of the tunnel flow on the effective camber shape and angle of attack of the airfoil.

The following analysis viewpoint is taken herein. It is desired to find an airfoil with angle of attack α_f and camber line z_f which would give the same pressure distribution in free unbounded flow as the airfoil in the tunnel at α_t with camber line z_t. This would allow the direct application of existing airfoil codes for this "free-equivalent" airfoil. From Ref. 5, for the case where the airfoil in the tunnel has zero-camber slope,

i.e., $dz_f/dx=0$ for the streamwise direction x,

$$\frac{z_f}{\alpha_t c}=\frac{-(1+2\sigma)}{\eta}\left(\frac{x}{c}\right)-\frac{4\sigma}{\eta}\left[\left(\frac{x}{c}\right)-\left(\frac{x}{c}\right)^2\right] \quad (1)$$

where

$$\eta=[(1+2\sigma)^2+\sqrt{12\sigma}]$$

and

$$\sigma=(\pi^2/48)(c/h)^2$$

The term c is the airfoil chord and h the tunnel "height" or vertical open-jet dimension for a horizontally aligned airfoil. Comparisons of Eq. (1) to more exact numerical solutions where no approximations are made based on the smallness of the ratios c/h and c/d, d being the distance to the jet nozzle exit, show excellent agreement. It is also of interest to define the angle that another airfoil in free unbounded flow (designated with an asterisk) with zero camber which would give the same lift as the airfoil in the tunnel. Again from Ref. 5

$$\alpha_*=\alpha_t/\eta \quad (2)$$

This angle for this "equilift" airfoil corresponds to the slope of the free-equivalent airfoil at $x/c=3/4$.

Sketches of the actual airfoil in the tunnel at angle α_t, the corresponding free-equivalent airfoil with its new camber line, and the equilift airfoil at angle α_* to unbounded flow are shown in Fig. 1.

Experiment

The data of this report are from hot-wire measurements of the boundary layer/near wake at the trailing edges of two-dimensional airfoil and flat-plate models. Testing parameters include model chord length (2.54-60.96 cm), flow velocity (23.8-71.3 m/s), angle of attack to flow, and boundary-layer turbulence through natural transition and tripping. Many of the details about the facility, procedures, and test models have been reported previously.[3] Key elements of the test, which have particular importance to the data presented herein, are given.

Method, Models, and Instrumentation

The models were tested in the low-turbulence potential core of a free jet, which was provided by a nozzle with rectangular exit dimensions of 0.3×0.46 m. Most of the models used are shown in Fig. 2. The two-dimensional models of concern here are all of 0.46 m span. The TE of each model was very sharp. For the NACA 0012 airfoils, the slope of the surface near the uncusped TE is 7 deg off the chordline. For the "flat plates" (maximum thickness of 3% of chord length c), the corresponding slope is 1.7 deg. The attached cylindrical hubs, shown on the models, allow flush-mounting to the two sideplates. The sideplates ($152\times30\times1$ cm) are themselves flush-mounted to the nozzle lips. For all models at a zero geometric angle of attack to the airflow, $\alpha_g=0$, the TE is located 61 cm above the nozzle exit. For the untripped cases (natural BL transition), the surfaces were kept very smooth and clean. For the tripped cases, the BL transition was achieved by a dense but nonoverlapping distribution of grit (nominal particle "diameter" of 0.29 mm) attached to the surface from the leading edge (LE) to 20% chord. This "heavy" trip was used to establish fully turbulent BLs for all models as guided by aeroacoustic requirements of the project.[3]

For the flow surveys, a computer-controlled traverse rig was used to position the hot-wire probes in the near wake. Figure 3 shows an example setup in the open tunnel. A three-dimensional case is shown so the model can be seen mounted to the sideplate. Upon defining an x axis to correspond to the chordline through the model's center with origin at the TE, the probes' traversing direction (z axis) was perpendicular to this. For data to follow, $x=0.64$ mm for the 2.54-cm-chord model and $x=1.3$ mm for all others. The probes were moved and signals averaged at discrete traverse positions. The hot-wire probes used include miniature cross-wire (0.5 mm distance between wire prongs) and single-wire types. For the cross-wire data, measured wire angle and on-site linearity calibrations were employed in the postprocessing. The single-wire results for a number of corresponding runs provided a final check of the cross-wire data calibration.

Finally, a concern of the testing configuration is a three-dimensional boundary-layer effect due to the potential flowfield interaction with the sideplates. For the zero-angle cases, this effect[3] is expected to be minimal as should be the case for the nonzero angles on the pressure side of the airfoils. The flow conditions on the suction side will have a three-dimensional character due to what may be described as a "turbulent-wedge" effect at the junctions of the airfoil and sideplates. This affects boundary-layer growth, but more so for the untripped cases than for the tripped ones due to the expected spanwise variation of transition for the larger-chord cases than for the small chords. However, in the data to follow

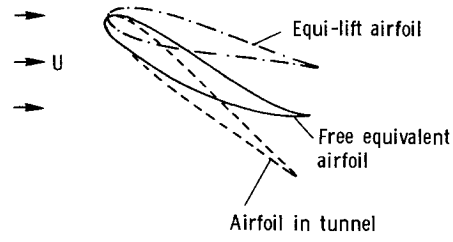

Fig. 1 Illustration of the airfoil in the tunnel and equivalent airfoils in the free field.

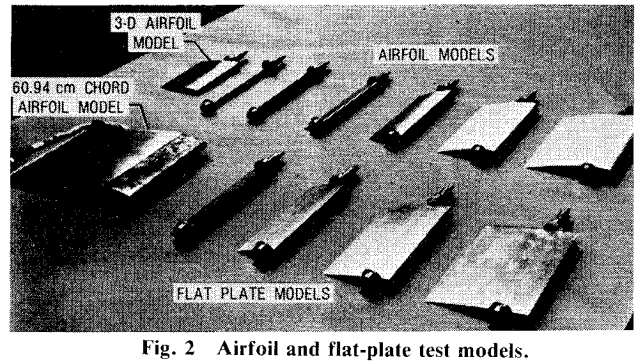

Fig. 2 Airfoil and flat-plate test models.

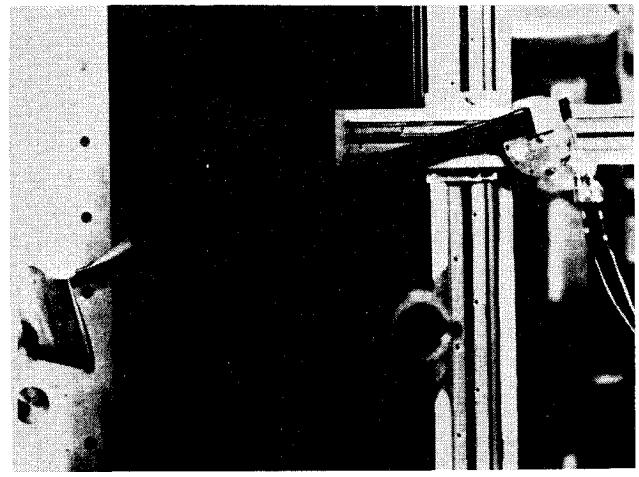

Fig. 3 Test setup for hot-wire measurement. A three-dimensional case is shown for clarity.

there is no apparent indication of any bias error due to the effect.

Parameter Determination

The integral parameters—displacement thickness δ^* and momentum thickness θ—are calculated from mean velocity profiles with the specification of the BL/near-wake thickness δ. The thickness δ is that distance from the airfoil surface where the mean velocity reaches 99% of the potential flow stream velocity. The values of δ were chosen based on detailed examinations[3] of the respective turbulent-velocity and Reynolds-stress distributions as well as the mean profiles. For all cases, the estimated accuracy of δ is within $\pm 5\%$ for the turbulent boundary-layer (TBL) flow and $\pm 10\%$ for laminar and transitional flows. For $\alpha = 0$ cases, these correspond to calculated deviations of ± 1.5 and $\pm 3\%$ for both δ^* and θ, respectively. For $\alpha > 0$ cases, mean-flow curvature in the trailing-edge region results in changes in the potential flowfield. This has the effect of increasing the sensitivity of the integral thickness calculations to the δ choices. Deviations in δ^* and θ become on the order of percent variations in δ.

For compatibility (to avoid bias errors) the single wire results presented for the $\alpha = 0$ cases were reprocessed to match the same z-axis resolution as the crosswire (0.5 mm). The resulting data scatter between the two types was found to be within about $\pm 7\%$ for both δ^* and θ. For the $\alpha \neq 0$ cases, only cross-wire data is presented for the larger models. For the two smaller chords (2.54 and 5.08 cm) for the untripped cases, and for the smallest chord for the tripped cases, only single-wire data are given because of the better z-axis resolution in these thin BLs. Additional discussion of error sources follows.

Trailing-Edge Flow Measurements

Velocity Profiles

Figure 4 shows distributions of mean and corresponding rms turbulent velocities U and u', respectively, of the TE flows normalized to the freestream velocity, $U_0 = 71.3$ m/s. The data are from single-wire probe surveys in the near wake of the two-dimensional airfoil and flat-plate models. The models were placed at $\alpha_f = 0$ deg so the distributions should ideally be symmetrical about the chordline which intersects the TE at $y = 0$. Results are presented for untripped flat plates of various chords in Fig. 4a. The boundary-layer flows are not symmetrical on opposing sides, indicating that the turbulence is not fully developed but is transitional in character. Slight physical variations between model sides can cause transition to begin at different chordwise locations. The larger chords with the higher Reynolds number transitioned earlier and are better developed. Figure 4b shows the same flat-plate conditions except the boundary-layer growth is enhanced by the artificial tripping. The fullness and the general similarity of the profiles are indicative of well-developed turbulent flows.

Airfoil-measured profiles are shown in Figs. 4c and 4d for the untripped and tripped cases, respectively. Comments similar to those for the flat plates can be made here for the airfoils with regard to the transitional characteristics for the un-

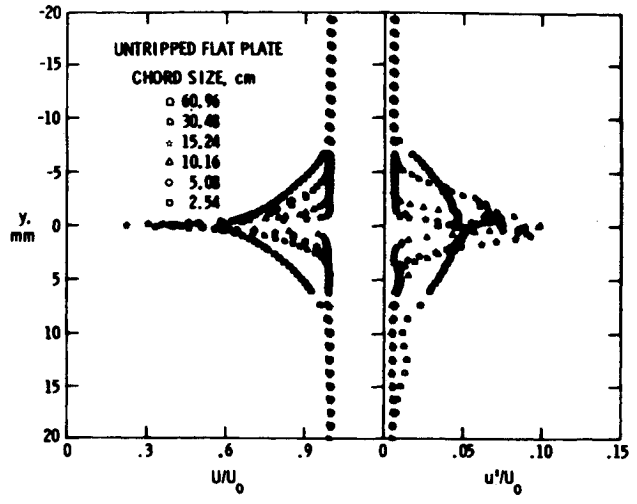

a) Flat plates with untripped BL.

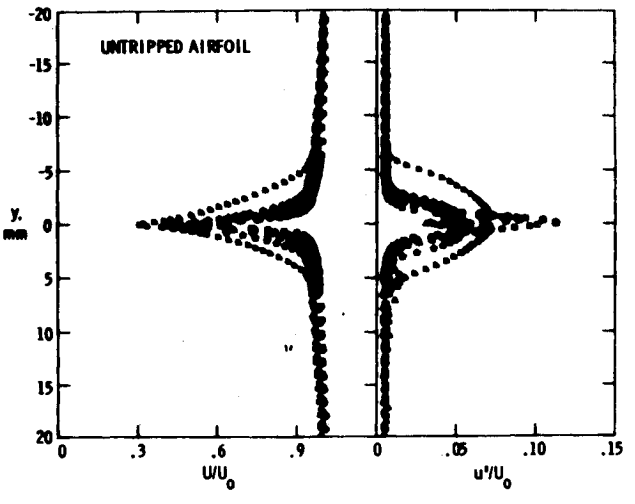

c) NACA 0012 airfoils with untripped BL.

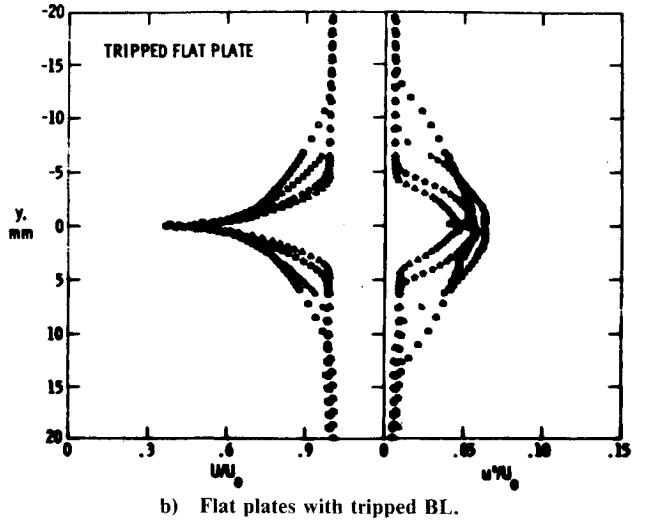

b) Flat plates with tripped BL.

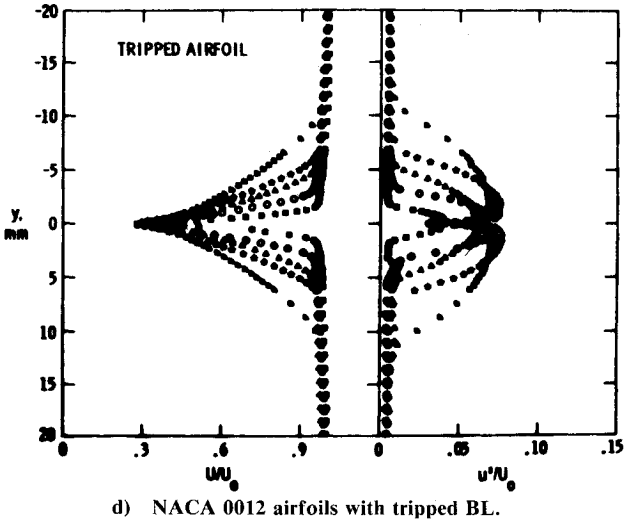

d) NACA 0012 airfoils with tripped BL.

Fig. 4 Mean and rms turbulent velocity profiles in the boundary layer/near-wake for different model types as a function of size for $\alpha_f = 0$ deg and $U_0 = 71.3$ m/s.

tripped cases and the more developed TBL flow for the tripped cases. Here, however, the airfoil shape and associated adverse pressure gradient, over most of the airfoil, result in a thicker and better developed TBL flow at the TE for all corresponding cases.

Profile data for the 10.16-cm-chord tripped airfoil at various angles of attack for $U_0 = 71.3$ m/s are shown in Fig. 5. The mean and turbulent velocities U and u' as well as the normalized turbulent Reynolds shear stress $-\overline{u'v'}/U_0^2$ and mean-flow direction $\phi = \tan^{-1}(V/U)$, where V is the mean vertical velocity, were determined from the cross-wire probes. For clarity, some spatial averaging was done to reduce the number of symbols. At $\alpha_t = 0$ the results show symmetry. The flow angle ϕ data does show that the boundary-layer/near-wake flow direction tends to conform to the 7 deg slope of the surface at the trailing edge. At small nonzero angles of attack the flow maintains its angularity with respect to the surface (note that $\phi = 0$ deg refers to the direction along the chordline regardless of α_t). At these small angles the velocity $U = U_e$ at the edge of the boundary layers increases only slightly. The thickness δ, as well as u'/U_0 and $-\overline{u'v'}/U_0^2$, decrease and increase, respectively, on the pressure and suction sides. At angles of attack large enough to see evidence of separation, the increases in the fluctuating quantities and the mean-flow angle ϕ are pronounced. The mean profile and angle data appear to indicate in the highly separated flow cases that, although the flow was highly skewed near the surface, the mean velocity vector was into the wake rather than upstream, showing no net flow reversal in the near wake. This was found to be the case for all models tested.

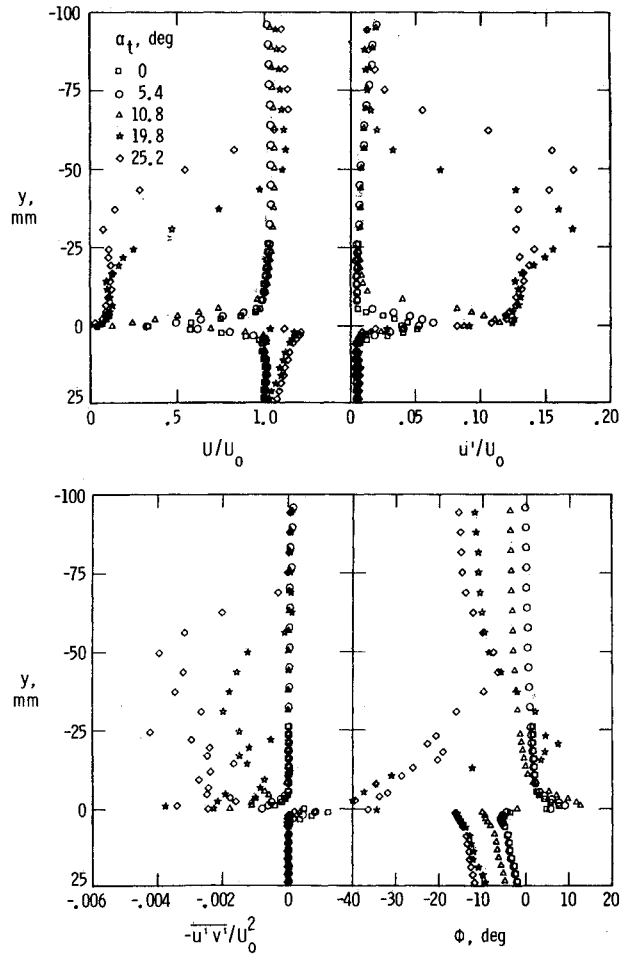

Fig. 5 Profile results for mean and rms turbulent velocity as well as turbulent shear stress and mean-flow angulation for tripped 10.16-cm-chord airfoil at various angles of attack α_t. $U_0 = 71.3$ m/s.

The flow velocities U_e increase with angle α_t at the edge of the boundary layers on both the airfoil sides by about the same amount, although the pressure side has higher U_e for the case of Fig. 5. For all angles for airfoils examined in this study it was found that $U_e/U_0 \approx 0.97 + 0.0011\alpha_*^2$ for the tripped cases and the constant 0.97 changed to 0.95 for the untripped cases. This is for both airfoil sides and within $\pm 2\%$ for most data. Other aspects of the profile data are presently discussed in context of the boundary-layer thickness parameter presentation.

Flat Plates at Zero Angle of Attack to the Flow

The thicknesses δ, integral properties δ^* and θ, and shape factors H ($= \delta^*/\theta$) at the trailing edge of the flat-plate models are given in Fig. 6 for both the artificially tripped and untripped cases. The parameters are normalized with chord and are given vs Reynolds number based on chord. Computed results using the Harris code[4] for the limiting cases of fully laminar boundary-layer flow and fully turbulent flow are shown.

The thickness data for the tripped boundary-layer cases are seen to lie above the predicted values. The trends, however, are indicative of fully turbulent flow. As mentioned, the surface roughness employed here for tripping is greater than the minimum required to complete transition. The effect is seen to move the "apparent" boundary-layer transition position upstream of the leading edge thereby producing the larger thicknesses.

In contrast to the tripped cases, the untripped data appear to be bounded from above and below by the limiting cases. Within this bracketing, a trend can be seen for every chord, which reveals information about the transition conditions of the tests. For the ideal low subsonic case with perfectly smooth inflow, all of the data should collapse along a single line from the laminar case to the fully turbulent one as a unique function of Reynolds number. However, the data show that transition

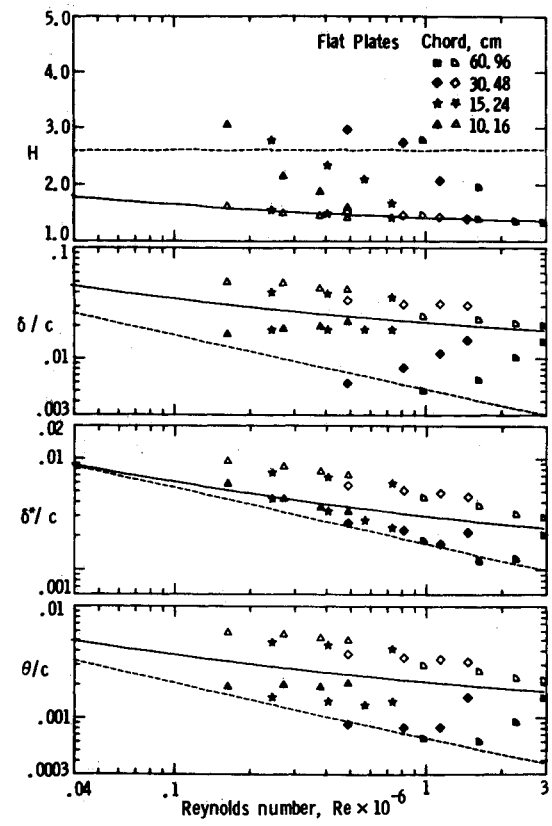

Fig. 6 Effects of Reynolds number for flat-plate data at $\alpha_t = 0$. ——: BL code with transition at leading edge; – – –: BL code with laminar boundary layer. Open symbols: tripped data; solid symbols: untripped data.

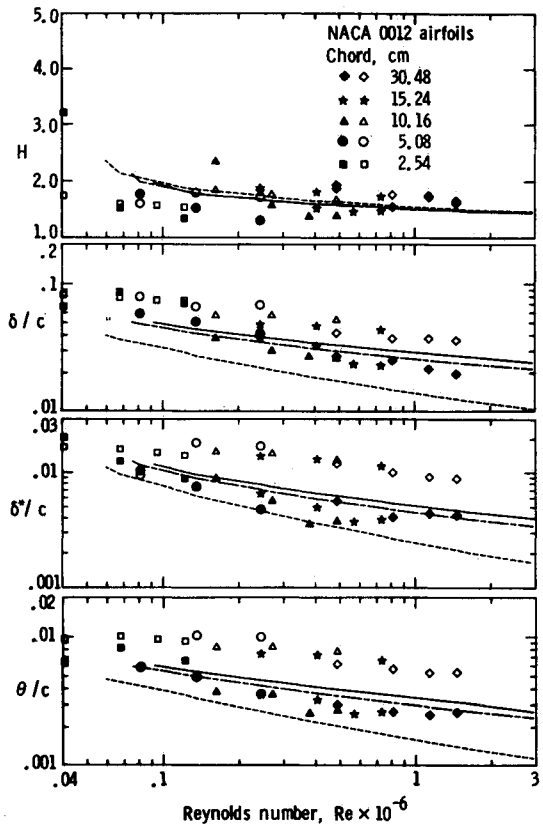

Fig. 7 Effects of Reynolds number for airfoil data at $\alpha_t = 0$ deg. —: BL code with transition at leading edge; – – –: BL code with transition 10% of chord before laminar separation. Open symbols: tripped data; solid symbols: untripped data.

from laminar to turbulent is really much more dependent on velocity than model Reynolds number per se. For each model, the boundary layers were essentially laminar at the trailing edge for the lowest speed, while at the highest speed the data show transition must have occurred near the leading edge. This is believed to be due to turbulence characteristics in the potential core of the free jet where the models were tested. It is known[7] that increasing stream turbulence intensity beyond about 0.05-0.1% leads increasingly to premature transition of boundary-layer flow. A review of hot-wire data obtained in the tunnel flow showed that the turbulence intensity increased with increases in freestream velocity. Near the model's trailing-edge positions $u'/U_0 = 0.10$, 0.35, 0.43, and 0.54% for the velocities $U_0 = 23.8$, 39.6, 55.5, and 71.3 m/s, respectively. This occurs in spite of the low turbulence intensity of about 0.03% at the center of the nozzle exit over a large range of velocities. The freestream turbulence at the model location is due apparently more to the close proximity of the developing turbulent shear layers of the free jet than the initial turbulence of the flow that leaves the nozzle. Such effects should be anticipated in all open wind-tunnel testing.

Based on the preceding testing concerns, little can be said (as expected) about transition criterion independent of tunnel effects. However, basic consistency of data and theoretical results for limiting cases are demonstrated.

Airfoils at Zero Angle of Attack

Figure 7 gives boundary-layer parameter results for the NACA 0012 models in the same format as for the flat plates of Fig. 6. The reference theory was computed based on transition to fully turbulent flow at the leading edge for one limiting case and at the 50% chord position (10% upstream of laminar separation) for another. Also shown is where transition is assumed to occur at the point of minimum pressure (12% chord).

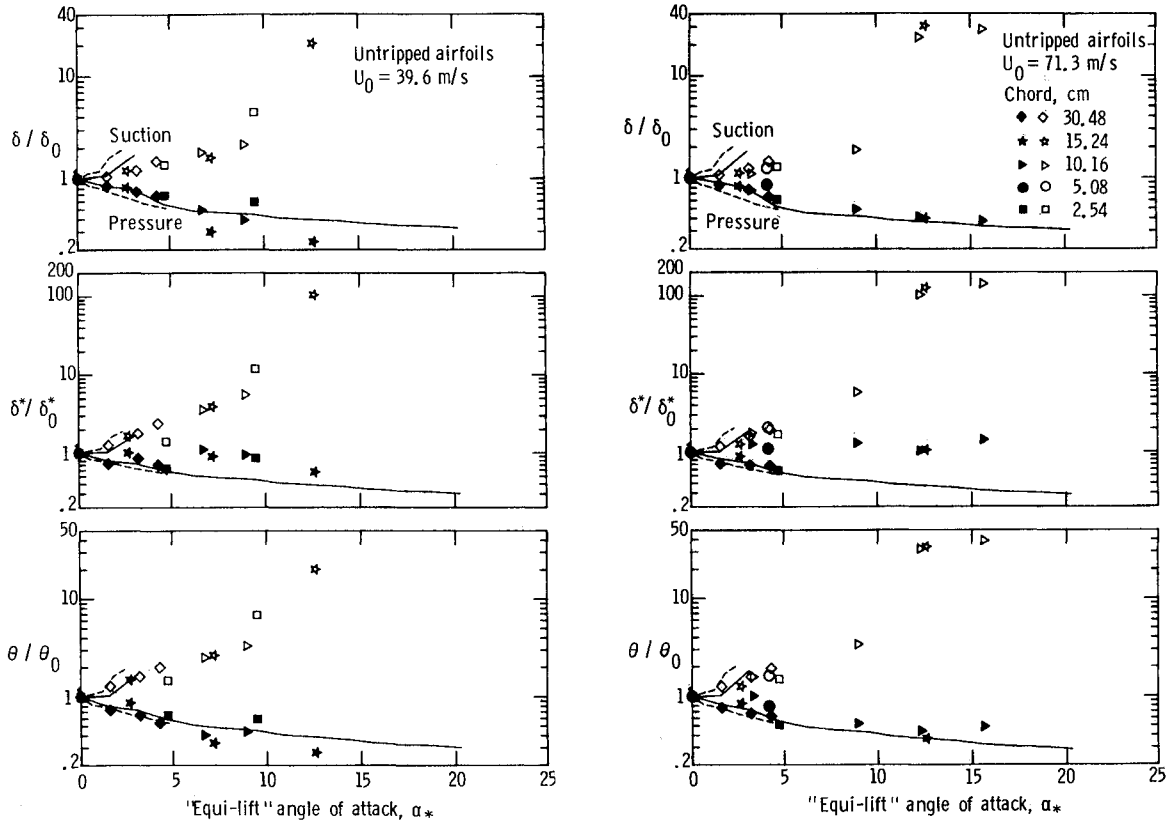

Fig. 8 Effects of angle of attack at two speeds for untripped airfoils. BL code for airfoils with lamiar or boundary-layer transition to turbulent near 10% before laminar separation. —: 5.08-cm chord; – – –: 30.48-cm chord. Open symbols: suction-side data; solid symbols: pressure-side data.

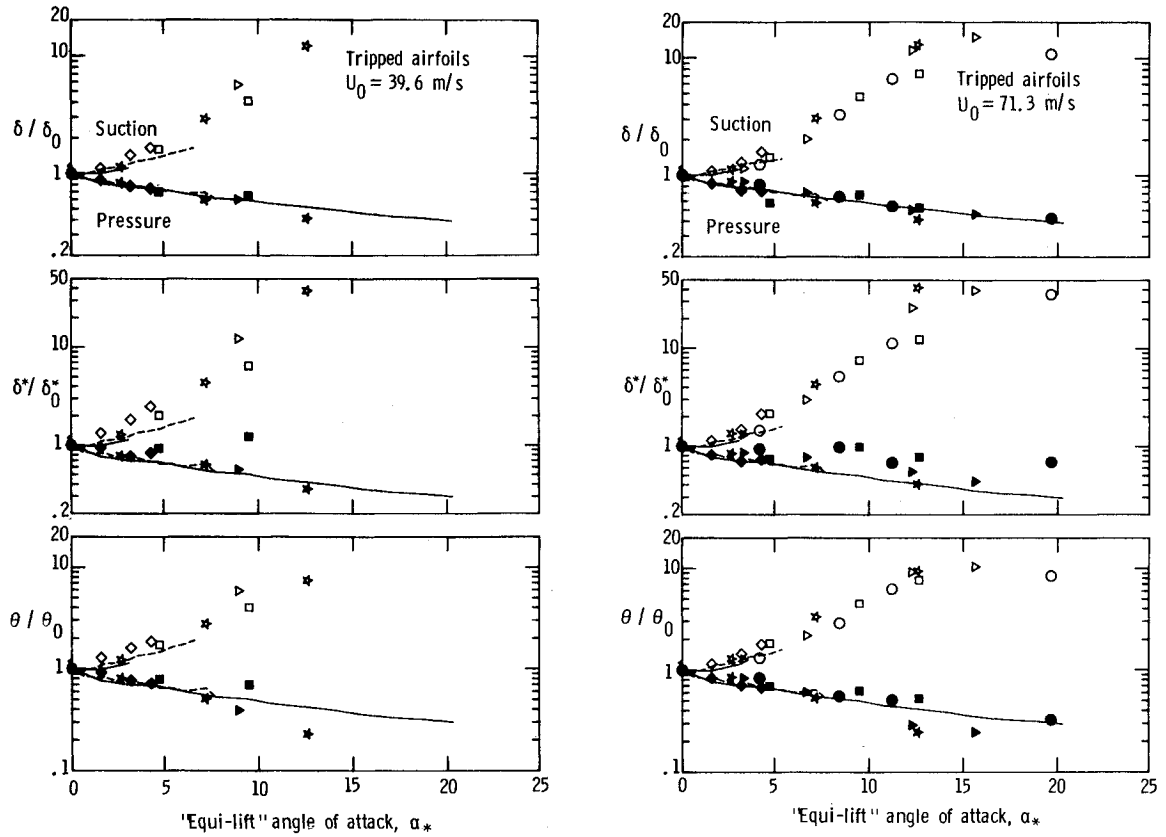

Fig. 9 Effects of angle of attack at two speeds for tripped airfoils. BL code for airfoils with transition at leading edge. ——: 5.08-cm chord; – – –: 30.48-cm chord. Open symbols: suction-side data; solid symbols: pressure-side data.

As with the flat-plate cases, the tripped data are scaled above the predicted fully turbulent lines due to the heavy tripping. Also, the untripped data are quite well bounded (or bracketed) by the values of the limiting cases, except the lowest Reynolds numbers considered. As was the case for the flat plate, the data in Fig. 7 should collapse to a single line assuming perfect inflow and surface similarity between models. For the untripped cases this again does not occur, apparently because of the inflow turbulence problem just discussed and its interaction with the pressure gradient effect. Particular transition models have not been attempted to explain the particular trends for the different chords. For the tripped cases, the inflow turbulence should have a minimal effect on the boundary-layer development. The apparent bias deviations observed for the tripped data for different chord sizes perhaps could be attributed to lack of geometric similarity since the tripping particle size was not varied along with the chord length.

Airfoils at Nonzero Angle of Attack

Angle-of-attack effects on the thickness parameters are given at freestream velocities of 71.3 and 39.6 m/s for the untripped and tripped airfoil cases in Figs. 8 and 9. The parameters are normalized by those measured for corresponding cases at zero angle of attack, as given in Fig. 7. The data are plotted vs the "equilift" angle α_* of Eq. (2). The collapse of the data is much improved over that when α_l is used. For the present data $\alpha_* = 0.88\alpha_l$, $0.78\alpha_l$, $0.62\alpha_l$, $0.50\alpha_l$, and $0.30\alpha_l$ for the 2.54-, 5.08-, 10.16-, 15.24-, and 30.48-cm chord models, respectively. In general, of course, the data show that for increasing angle α_* (or α_l) the thicknesses increase on the suction side due to the increasing severity of the adverse pressure gradient. The converse is true for the pressure side where the pressure gradient becomes increasingly favorable.

Compared to the untripped data in Fig. 8 some predictions are computed assuming transition at 10% upstream of laminar separation as was described for Fig. 7. The reference theory is for one small and one large chord case for each velocity. The corresponding tripped boundary-layer cases are given in Fig. 9. The theory here, as in the previous figures, is presented to the extent that the flow does not separate in the computations prior to reaching the trailing edge. Even though flow separation occurs at fairly low α_* angles, the experimental suction-side measurements show agreement between the different models over a large range of α_* angles. On the pressure side, both δ and θ agree well with the predicted values, although δ^* does not at the higher values of α_*.

A discussion of error sources for Figs. 8 and 9 for the data as well as the reference theory is in order. First, since the theoretical profiles are calculated exactly at the TE, the velocity profile goes to zero at $z = 0$, while the measured data show some fill-in of the near-wake velocity defect profile. This is seen in Fig. 5a. The effect of the fill-in is worsened by flow curvature in the near wake for these nonzero angle-of-attack cases, as well as by cross-wire probe resolution limitations. With regard to theoretical errors, the particular inviscid potential code used to generate the pressure distributions does not consider the displacement of the streamlines due to the boundary layer. This gives approximate pressure distributions which produce lower than actual values for U at the boundary-layer edge. With the presence of flow separation on the suction side, as shown in Fig. 5, some difficulties described previously are evident. The flow is severely curved, making it difficult to select the minimum velocity point for the calculations of δ^* and θ. The boundary layer on the pressure side is very thin, which aggravates resolution limitations related to the finite size of cross-wire probes.

The preceding may explain much of the disagreement on the pressure side for Figs. 8 and 9 since the errors tend to increase the δ^* data while the incorrect pressure distributions make the numerical calculations too low. An additional point is that the thickness parameters were determined from available data

with the assumption that the mean-flow profile is for velocity oriented along the positive x direction ($\phi = 0$ deg) in Fig. 5b. While this leads to negligible error for attached and mildly separated flow, substantial separation, such as that for the two largest angles of Fig. 5, shows angles ϕ beyond 20 deg where more error can be introduced. This is a limitation one should recognize when utilizing the separated boundary-layer data.

A concluding point about Figs. 8 and 9 is that the use of the equilift angle α_* in presenting the thickness results represents in itself the first-order correction for open wind-tunnel effects. The predictions shown include the higher-order corrections, which incorporate the aerodynamically effective changes in camber due to the tunnel. The extent to which the predictions differ are representative of the importance of the effective camber changes on the expected development of the airfoil's boundary layer.

Conclusion

Near-wake flow data are reported for a number of two-dimensional sharp, trailing-edge models. For the ideal low-Mach-number case of perfectly smooth inflow conditions and model similarity, boundary-layer thickness parameters should scale as unique functions of Reynolds number. This was not found to be the case for either the flat plate or airfoil models due to apparent boundary-layer transitional behavior not totally controlled by local Reynolds number conditions. The tunnel inflow turbulence intensity, and the likely presence of strong pseudosound pressure, incident on the models apparently caused earlier transition for the higher velocity cases. For the tripped cases, where inflow conditions should not materially affect boundary-layer development, the data deviation from pure Reynolds number dependence is likely due to lack of geometric similarity. The trip grit size was not varied to correspond to model size. Boundary layers for the smaller chords were thicker relative to the chord size.

The inclusion of boundary-layer computations for comparison permits some assessment of prediction capabilities, when given only nominal geometry and flow conditions as theoretical input, and of the importance of wind-tunnel corrections to the predictions. It also provides some understanding of the boundary-layer transition behavior which has implications about the open wind-tunnel test environment. The untripped data is clearly bracketed by the reference theory. The prediction code curves correspond to limiting assumptions about transition locations. This establishes confidence limits for predictions independent of any transition criteria. The results also indicate that both the angle-of-attack and camber corrections are important in the boundary-layer calculations, although the angle of attack corrections were by far more important in the comparisons.

References

[1] Patel, V.C. and Scheverer, G., "Calculation of Two-Dimensional Near and Far Wakes," *AIAA Journal,* Vol. 20, July 1982, pp. 900-907.

[2] Viswanath, P.R., Cleary, J.W., Seegmiller, H.L., and Horstman, C.C., "Trailing-Edge Flows at High Reynolds Number," AIAA Paper 79-1503, July 1979.

[3] Brooks, T.F. and Marcolini, M.A., "Airfoil Self Noise—Effect of Scale," AIAA Paper 83-0785, 1983; also, "Scaling of Airfoil Self-Noise Using Measured Flow Parameters," *AIAA Journal,* Vol. 23, Feb. 1985, pp. 207-213.

[4] Harris, J.E. and Blanchard, D.K., "Computer Program for Solving Laminar, Transitional, or Turbulent Compressible Boundary-Layer Equations for Two-Dimensional and Axisymmetric Flow," NASA TM-83207, Feb. 1982.

[5] Brooks, T.F., Marcolini, M.A., and Pope, D.S., "Airfoil Trailing Edge Flow Measurements and Comparison with Theory Incorporating Open Wind Tunnel Corrections," AIAA Paper 84-2266, Oct. 1984.

[6] Zorumski, W.E., "Aircraft Noise Prediction Program Theoretical Manual," NASA TM-83199, Feb. 1982.

[7] Schlichting, H., *Boundary Layer Theory,* 6th Ed., McGraw-Hill Book Co., New York, 1968.

[8] Spence, D.A., "Prediction of the Characteristics of Two-Dimensional Airfoils," *Journal of the Aeronautical Sciences,* Vol. 21, Sept. 1954, pp. 577-587.